RSC Advances

ROYAL SOCIETY OF CHEMISTRY

www.rsc.org/advances

Efficient photocatalytic degradation of bisphenol A and dye pollutants over $BiOI/Zn_2SnO_4$ heterojunction photocatalyst

Tao Yan,[a,b] Hongye Liu,[c] Meng Sun,[a] Xiaodong Wang,[c] Mengmeng Li,[c] Qing Yan,[a] Wenguo Xu,[b] and Bin Du*[a]

[a] School of Resources and Environment, University of Jinan, Shandong Provincial Engineering Technology Research Center for Ecological Carbon Sink and Capture Utilization, Jinan250022, P.R. China. Fax: +86 531-82765969; Tel:+86 531-82769235; E-mail: binduujn@163.com

[b] School of Chemistry, Beijing Institute of Technology, Beijing 100081, P.R. China.

[c] School of Civil Engineering and Architecture, University of Jinan, Jinan 250022, P.R. China.

Graphical abstract

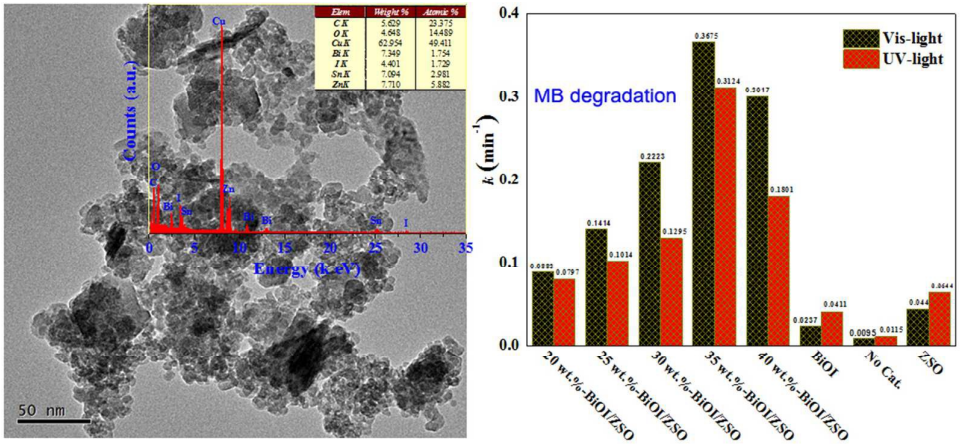

The formation of heterojunction between BiOI and Zn_2SnO_4 greatly enhanced the photocatalytic activity of $BiOI/Zn_2SnO_4$ composites.

Cite this: DOI: 10.1039/c0xx00000x

www.rsc.org/xxxxxx

ARTICLE TYPE

Efficient photocatalytic degradation of bisphenol A and dye pollutants over BiOI/Zn_2SnO_4 heterojunction photocatalyst

Tao Yan,[a,b] Hongye Liu,[c] Meng Sun,[a] Xiaodong Wang,[c] Mengmeng Li,[c] Qing Yan,[a] Wenguo Xu,[b] and Bin Du*[a]

Received (in XXX, XXX) XthXXXXXXXXX 20XX, Accepted Xth XXXXXXXXX 20XX
DOI: 10.1039/b000000x

Abstract: BiOI/Zn_2SnO_4 composites with heterostructure have been synthesized via a chemical deposition method under mild conditions by tuning the BiOI mass ratios. The physicochemical characteristics were investigated by X-ray diffraction pattern (XRD), diffuse reflectance ultraviolet–visible light spectra (DRS), scanning electron microscopy (SEM), and high-resolution transmission electron microscopy (HRTEM). The XRD results show that two phases of BiOI and Zn_2SnO_4 were co-existed in the composites. The HRTEM image showing clear lattice fringes proves the formation of heterojunction at the interfaces of BiOI and Zn_2SnO_4. The photocatalytic degradations of endocrine disruptor bisphenol A and dyes (MB and RhB) indicated that the BiOI/Zn_2SnO_4 composites were more photoactive than pure BiOI and Zn_2SnO_4. The activity enhancement was mainly ascribed to the formation of heterojunction between BiOI and Zn_2SnO_4, which facilitated the transfer and separation of photogenerated electron-hole pairs. The photoelectrochemical measurement has also confirmed the enhancement of separation efficiency of electron–hole pairs.

Keywords: BiOI/Zn_2SnO_4; Photocatalysis; Heterostructure; UV and visible light; Bisphenol-A

Introduction

Heterogeneous photocatalysis has become an exciting and rapidly growing research area in the last few years [1,2]. Photocatalysis technology can be used to decompose organic compounds into inorganic substances efficiently and completely under mild conditions, so it has a great application prospect for purifying industrial wastewater [3,4], or splitting water into hydrogen and oxygen gases for clean renewable energy [5]. There are numerous papers on the photodegradation of organic compounds, and the reported photocatalysts mainly include oxides, nitrides, sulfides, etc., but most of them are focused on TiO_2-based photocatalyst [6,7]. As classic photocatalyst, TiO_2 has a low quantum yield, poor solar energy utilization, and severe deactivation, which greatly limits the application. So, to develop novel non-TiO_2 based photocatalysts, which were environmental friendly and highly efficient has become the focus of photocatalysis research. The n-type Zn_2SnO_4 semiconductor which is composed of the d^{10} *p*-block metal ion has potential applications in photoelectrical devices, batteries, functional coatings, and photocatalysis due to its high electron mobility and high electrical conductivity [8-12]. Owing to its wide band-gap, Zn_2SnO_4 can only utilize a small fraction of solar light. In order to expand its optical response from the UV to visible light region and improve the separation efficiency of photo-generated carriers, narrow band gap semiconductors have been used to combine with it. Semiconductor coupling not only extend the light absorption range but also promote the photo-induced carriers separation efficiency, which ultimately result in excellent photocatalytic activity [13]. In the past few years, the heterojunction fabricated by semiconductor coupling has also been used to prepare novel catalysts, such as Bi_2O_3/Bi_2S_3 [14], g-$C_3N_4/Bi_2O_2CO_3$ [15], g-C_3N_4/BiOX (X = Br, I) [16-17], $Bi_2O_3/BiVO_4$ [18], and $Bi_2O_2CO_3$/BiOI [19] have been developed for effective visible light driven photocatalyst.

Recently, BiOI has drawn extensive interests of researchers because of its unique electrical and optical properties [20-22]. As a typical p-type semiconductor, BiOI has been naturally selected to couple with n-type TiO_2 [23, 24], $ZnSn(OH)_6$ [25], $ZnTiO_3$ [26] and ZnO [27] etc. Likewise, Fan and co-workers [28] reported the synthesis of p-BiOI/n-Zn_2SnO_4 heterostructures with photocatalytic activity for the degradation of MO under visible light irradiation, but the activity was still not very well. Thus, it pushes us to thoroughly investigate the synthesis and activity enhancement of BiOI/Zn_2SnO_4 with heterostructure.

Herein, we report the characterization and photocatalytic properties of BiOI/Zn_2SnO_4 composite prepared by a facile and economical two-step method. Zn_2SnO_4 nanoparticles were first

[a] *School of Resources and Environment, University of Jinan, Shandong Provincial Engineering Technology Research Center for Ecological Carbon Sink and Capture Utilization, Jinan250022, P.R. China. Fax: +86 531-82765969; Tel:+86 531-82769235; E-mail: binduujn@163.com*
[b] *School of Chemistry, Beijing Institute of Technology, Beijing 100081, P.R. China.*
[c] *School of Civil Engineering and Architecture, University of Jinan, Jinan 250022, P.R. China.*

prepared by solvothermal method, and then, the BiOI/Zn_2SnO_4 composites were prepared by chemical deposition method under mild conditions. The photocatalytic activity and recycling ability were investigated by the degradation of dye pollutants (MB, RhB) and endocrine disruptor bisphenol A (BPA) under UV and visible light irradiation, respectively. The degradation efficiency of pollutants over BiOI/Zn_2SnO_4 composites was greatly enhanced compared with that over pure Zn_2SnO_4 or BiOI. This activity enhancement was mainly ascribed to the formation of heterojunction at the interface of BiOI and Zn_2SnO_4, which facilitated the transfer and separation of photo-generated carriers, as well as the strong visible light absorption originating from the sensitization role of BiOI to Zn_2SnO_4.

Experimental section

Synthesis of Zn_2SnO_4 precursor

All chemicals with analytical purity were obtained from Sinopharm Chemical Reagent Co., Ltd and were used without further purification. Deionized water was employed in all experiments. In a typical procedure for the synthesis of Zn_2SnO_4, 2.10 g $ZnCl_2$ and 2.70 g $SnCl_4{\cdot}5H_2O$ were added to 100 mL water/ethylene glycol=1:1 (volume ratio) under magnetic stirring. Then 50 mL of 2 M *n*-butylamine aqueous solution was added dropwise to the above solution. The final concentration of *n*-butylamine in the solution was 0.4 M. After stirring for 30 min, the obtained white slurry was transferred to 100 mL autoclave and maintained at 180 °C for 20 h. The product formed at the bottom of the autoclave was centrifuged and rinsed thoroughly with deionized water and ethanol several times. Finally, the product denoted as ZSO was dried in air at 60 °C for 6 h.

Preparation of BiOI/Zn_2SnO_4 composites

The BiOI/Zn_2SnO_4 samples with different BiOI contents were prepared by a deposition method. In a typical experiment, different stoichiometric amounts of $Bi(NO_3)_3{\cdot}5H_2O$ and KI were dissolved in 20 mL ethylene glycol to obtain a clear solution A. Zn_2SnO_4 was ultrasonically dispersed into 80 ml deionized water to form a homogeneous solution B. Then, the solution A was added drop-wise into the solution B under strong stirring. After being stirred for 1.0 h at room temperature, the resulting mixtures were heated at 80 °C for 2.0 h in an oil bath. Finally, the precipitates were collected, washed thoroughly with deionized water and ethanol, and dried at 60°C in air. According to this method, BiOI/Zn_2SnO_4 composites with different mass ratios of 20, 25, 30, 35, and 40 wt% have been synthesized and named as BiOI/ZSO-20, BiOI/ZSO-25, BiOI/ZSO-30, BiOI/ZSO-35, and BiOI/ZSO-40, respectively. For comparison, pure BiOI was prepared by adopting the method in the absence of Zn_2SnO_4.

Characterization of photocatalysts

X-ray diffraction (XRD) patterns of the obtained products were recorded on a Bruker D8 Advance X-ray diffractometer under the conditions of generator voltage = 40 kV; generator current = 40 mA; divergence slit = 1.0 mm; Cu Kα (λ = 1.5406 Å); and polyethylene holder. The morphologies and microstructures of the samples were examined with a Hitachi S-4800 scanning electron microscopy (SEM). The transmission electron microscopy (TEM) and high-resolution transmission electron microscopy (HRTEM) images were measured by a JEOL model JEM 2010 EX instrument at an accelerating voltage of 200 kV. Carbon-coated copper grid was used as the sample holder. Energy-dispersive X-ray spectra (EDS) were obtained on a JEOL-2010 at an accelerating voltage of 200 kV. Diffuse reflectance ultraviolet–visible light spectra (DRS) were measured at room temperature in the range of 200–700 nm on a UV–vis spectrophotometer (Cary 500 Scan Spectrophotometers, Varian, and U.S.A) equipped with an integrating sphere attachment.

Photocatalytic tests

Photocatalytic reactions were acted in a customized reactor with a cooling-water-cycle system. It can keep the reaction temperature of the aqueous solution to maintain at room temperature. The visible light activity of BiOI/Zn_2SnO_4 composites were evaluated by photo-degradation of dyes and BPA in aqueous solution using a 300 W xenon lamp (PLS-SXE300C, Beijing Perfect Light Co. Ltd., Beijing) with a cutoff filter (λ > 420 nm) as light source. The UV light activities of BiOI/Zn_2SnO_4 composites were tested using four 4 W UV lamps with a wavelength centered at 254 nm (Philips, TUV 4W/G4 T5) as the light source. In each experiment, 100 mg of photocatalyst was added into 100 mL dye (MB and RhB) solution (10 mg/L) or BPA solution (20 mg/L). Before irradiation, the suspensions were magnetically stirred in dark for 60 min to ensure the establishment of an adsorption/desorption equilibrium. During reaction under light irradiation, 3 mL of suspension was sampled at given time intervals and centrifuged to remove the photocatalyst particles. The resulting clear liquor was analyzed on a Perkin-Elmer UV-vis spectrophotometer (Model: Lambda 35) to record the concentration changes of pollutant solution.

Photocurrent measurements (PC)

The photoelectrochemical experiment was conducted on CHI 760E electrochemical workstation (CHI 760E Chenhua Instrument Company, Shanghai, China) in a conventional three-electrode configuration with a Pt wire as the counter electrode and a saturated calomel electrode as reference electrode. Irradiation proceeded by a Xe arc lamp through a UV cut off filter (λ > 420 nm). Na_2SO_4 (0.2 M) aqueous solution was used as the electrolyte. The working electrodes were prepared as follows: An indium tin oxide (ITO) glass piece with a size of 2.0 × 1.0 cm. Then ITO glass piece was cleaned successively by acetone, ethanol, deionized water, and then dried in N_2 stream. 5.0 mg of the ground sample was dispersed uniformly with 1.0 mL of distilled water under the condition of ultrasonic, and 10 μL of above solution was added to surface of the ITO, and then 5 μL of Nafion solution (0.5 %) was dropping added on the modified working electrode surface as binder and dried at 120 °C for 1 h.

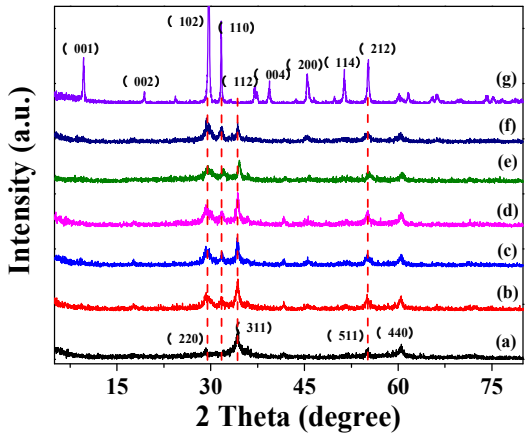

Figure 1. XRD patterns of (a) pure Zn_2SnO_4, (b) BiOI/ZSO-20, (c) BiOI/ZSO-25, (d) BiOI/ZSO-30, (e) BiOI/ZSO-35, (f) BiOI/ZSO-40, and (g) pure BiOI.

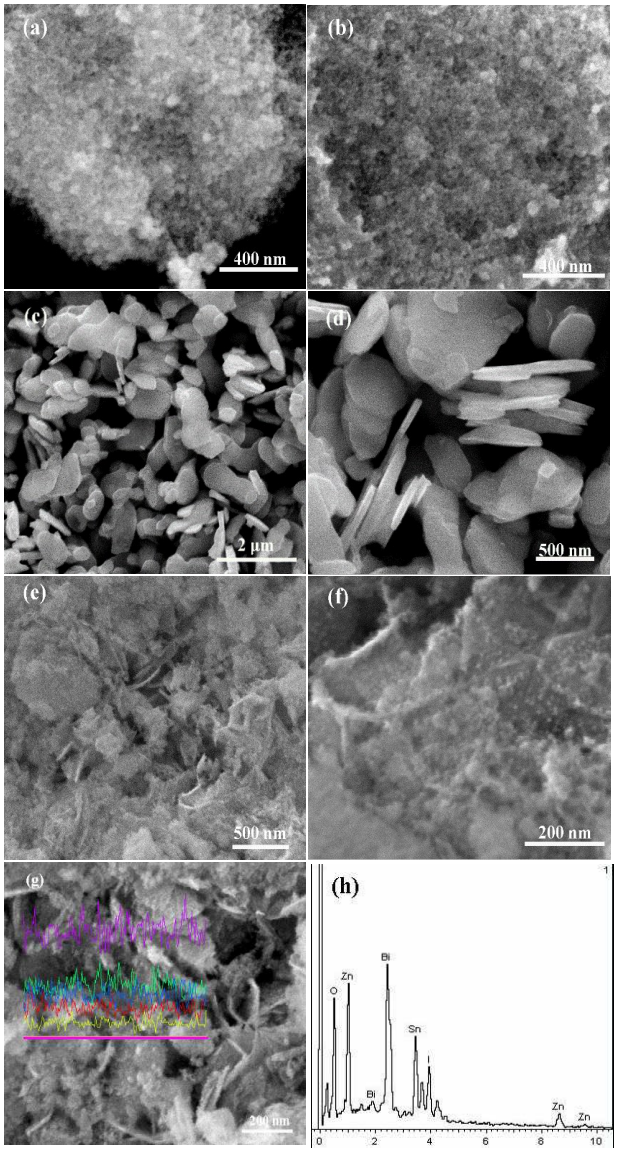

Figure 2. SEM images of (a)-(b) pure Zn_2SnO_4; (c)-(d) pure BiOI; (e)-(f) BiOI/ZSO-35; (g) The EDS line-scans image of BiOI/ZSO-35; (h) The EDS spectrum of BiOI/ZSO-35.

Results and discussion

Structural characterization

Figure 1 shows the XRD patterns of pure BiOI, Zn_2SnO_4, and BiOI/Zn_2SnO_4 composites with different mass ratios. As we can see, all the diffraction peaks in Figure 1a could be indexed to the tetragonal phase of BiOI (JCPDS no. 73-2062) [29] while that for Zn_2SnO_4 was the cubic phase (JCPDS no. 74-2184) [30]. The sharp and intense diffraction peaks of BiOI and Zn_2SnO_4 indicated that the samples were well crystallized. For the BiOI/Zn_2SnO_4 composites (Figure 1b-f), characteristic peaks for BiOI and Zn_2SnO_4 were both observed. Notably, the peaks assigned to BiOI became broader and weaker, suggesting that the presence of Zn_2SnO_4 could inhibit the crystal growth of BiOI [31]. In addition, no other impurity peaks have been found from the diffraction patterns, indicating that the composites are only composed of BiOI and Zn_2SnO_4.

The morphologies of Zn_2SnO_4, BiOI and BiOI/Zn_2SnO_4 composites have been characterized by SEM. As shown in Figure 2, the pure Zn_2SnO_4 presents irregular aggregates of uniform nanoparticles with the diameter of approximately 5-10 nm, as reported by Kim et al. [32]. It also reveals that the pure BiOI was consisted of large number of irregular plates with smooth surfaces. As for the BiOI/ZSO-35 sample, it obviously shows that the Zn_2SnO_4 nanoparticles are uniformly embedded in the BiOI plates (Figure 2e-f). Meanwhile, the morphology of BiOI nanoplate changed obviously after the addition of Zn_2SnO_4 nanoparticles, further revealing that the addition of Zn_2SnO_4 significantly affects the morphologies and crystal growth of BiOI, which is consistent with the XRD analysis. A similar phenomenon has also been reported by Zhang et al. [31]. Figure 2g presents the typical EDS line scanning results. It indicates that the elements of Bi, O, I, Sn and Zn are uniformly distributed across the scanned distance. Figure 2h displays the EDS spectrum for the as-prepared sample. It can be seen that only Bi, O, I, Sn and Zn elements existed in the composite, demonstrating that BiOI/ZSO-35 composite was composed of both BiOI and Zn_2SnO_4.

In order to further ascertain the formation of heterojunction between BiOI and Zn_2SnO_4, the sample was further investigated by TEM and HRTEM. Figure 3a shows the typical TEM image of BiOI/Zn_2SnO_4 composite, in which Zn_2SnO_4 nanoparticles were deposited on the surface of the plate-like BiOI substrates, it was consistent with the SEM observations. A magnified TEM image (Figure 3b) reveals that some nanoparticles with sizes of about 7 nm are anchored on the plates. Figure 3c presents the HRTEM image of the BiOI/Zn_2SnO_4 composite, the clear lattice fringes reveal that the materials are highly crystallized. Two sets of different lattice images are observed with *d* spaces of 0.28 and

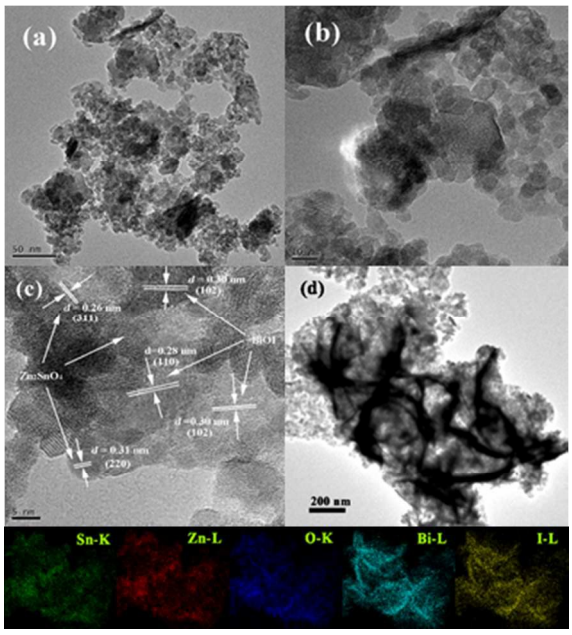

Figure 3. (a)-(b) TEM and (c) HRTEM images of the BiOI/ZSO-35 composite, and (d) the corresponding EDS mapping images of Zn, Sn, O, Bi and I elements.

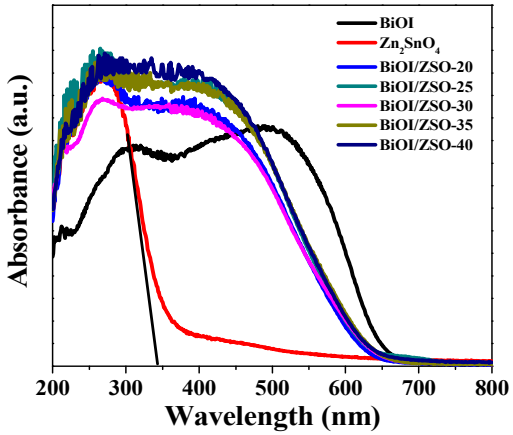

Figure 4. UV–vis diffuse reflectance spectra of Zn_2SnO_4, BiOI and BiOI/Zn_2SnO_4 composites.

0.30 nm corresponding to the (1 1 0) and (1 0 2) plane of tetragonal BiOI [33], and with *d* spaces of 0.26 and 0.31 nm belonging to the (3 1 1) and (2 2 0) planes of Zn_2SnO_4 [28], respectively. The HRTEM analysis demonstrated that the existence of BiOI/Zn_2SnO_4 heterojunction. These results are in good accordance with the XRD results. And the corresponding EDS mapping images (Figure 3d) of Zn, Sn, O, Bi and I elements further demonstrated that these elements distribute uniformly all through the composites.

Optical characterization

The optical absorption properties of Zn_2SnO_4, BiOI, and BiOI/Zn_2SnO_4 composites are shown in Figure 4. The absorption edges of Zn_2SnO_4 and BiOI were roughly located at 345 and 670 nm, respectively. When Zn_2SnO_4 combines with different amounts of BiOI, the optical absorption edges shifted from 345 to 650 nm. It has been reported that the inhibited recombination between photoelectrons and holes could result in the strong response in the visible region [34-35]. Moreover, the steep shape of the spectrum indicated that the visible light absorption was due to the band gap transition. The band gap energy of a semiconductor could be calculated by the following equation [36]:

$$\alpha h\nu = A(h\nu - E_g)^{n/2}$$

where α, *A*, ν and E_g are the absorption coefficient, a constant, light frequency and band-gap energy, respectively. Among them, *n* depends on the characteristics of the transition in a semiconductor (direct transition: $n = 1$; indirect transition: $n = 4$). For pure BiOI and Zn_2SnO_4, the value of *n* is 4 [37] and 1 [38], respectively. The band gap energies of the BiOI and Zn_2SnO_4 can be estimated from the plots of $(\alpha h\nu)^2$ or $(\alpha h\nu)^{1/2}$ versus photon energy ($h\nu$), respectively. Figure S1 shows that the calculated band gaps (E_g) of Zn_2SnO_4 and BiOI is 3.59 and 1.85 eV, respectively.

Photocatalytic activity

The photocatalytic activities of BiOI/Zn_2SnO_4 composites were first investigated by the degradation of MB (10 mg/L). Figure 5a shows the degradation of MB over Zn_2SnO_4, BiOI, and BiOI/Zn_2SnO_4 composites under visible (λ > 420 nm) light irradiation. As we can see, MB degradation was not observed in the dark condition. However, in the absence of any photocatalyst, the concentrations of MB showed a little decrease under visible

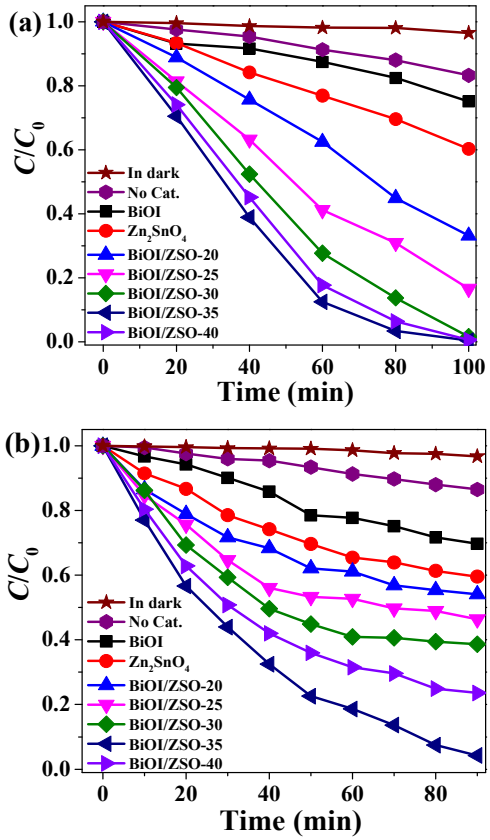

Figure 5. Photocatalytic activities of Zn_2SnO_4, BiOI and BiOI/Zn_2SnO_4 composites for the degradation of MB (10 mg/L) under (a) visible (λ > 420 nm) light and (b) UV (λ = 254 nm) light irradiation.

light irradiation. It is noteworthy that the MB decomposition over pure Zn_2SnO_4 has also been observed under visible light

irradiation (Figure 5a). This phenomenon may be ascribed to the weak dye photosensitization role of MB [39]. When $BiOI/Zn_2SnO_4$ composites were added, the degradation rates of MB were significant improved compared with that over pure BiOI and Zn_2SnO_4. Furthermore, the BiOI content contributes great influences on the photocatalytic activities of $BiOI/Zn_2SnO_4$ composites. Concretely, the photocatalytic activities were first remarkably enhanced along with the increasing of BiOI content, when the BiOI content was larger than 35%, the activities would decrease gradually, suggesting that the optimal BiOI mass ratio in $BiOI/Zn_2SnO_4$ composite was 35wt.%. Under the optimum conditions, nearly 100% of MB could be decomposed within 100 min under visible light irradiation. The photocatalytic degradations of MB under UV light (254 nm) irradiation have also investigated, and a very similar phenomenon has been observed. As shown in Figure 5b, the BiOI content also greatly influenced the UV activities of $BiOI/Zn_2SnO_4$ composites, and the BiOI/ZSO-35 sample exhibited the best activity. Under UV light irradiation, nearly 100% of MB could be decomposed within 90 min of reaction. As a comparison, the degradation of MB over PM-BiOI/ZSO-35 (the physical mixture of BiOI and Zn_2SnO_4, Labeled as PM-BiOI/ZSO-35) and BiOI/ZSO-R (prepared according the Ref. 28) was also investigated under the same conditions, and the degradation results were shown in Fig. S1. As we can see, whatever under UV or visible light irradiation, the activity of PM-BiOI/ZSO-35 is getting worse compared with that of BiOI/ZSO-35. Besides, the degradation rates of MB over BiOI/ZSO-35 was remarkably enhanced compared with BiOI/ZSO-R. The enhancement of photocatalytic activity could be attributed the synergetic effects of light absorption and heterojunction structure of $BiOI/Zn_2SnO_4$. It has also been found that the photocatalytic degradation of MB dye followed the first-order kinetics, and the kinetic constant (k) values were shown in

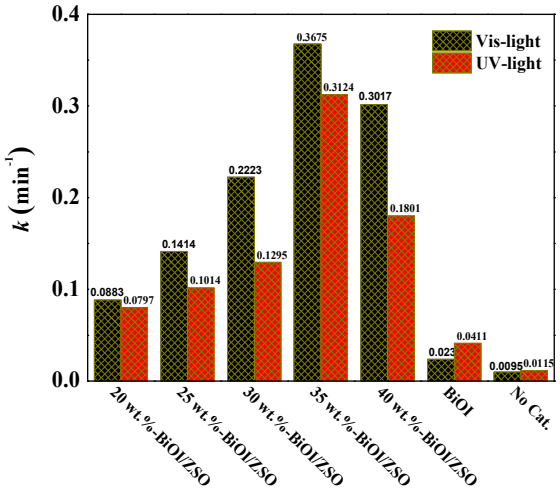

Figure 6. Photocatalytic degradation rate constant k of MB as a function of BiOI content (wt.%) under visible ($\lambda > 420$ nm) light and UV ($\lambda = 254$ nm) light irradiation.

Figure 6. As we can see, whatever under UV or visible light irradiation, the BiOI content greatly affected the kinetic constant k. It reaches the maximum value when the mass ratio of BiOI was 35%. The kinetic constant k of BiOI/ZSO-35 under UV and visible light irradiation is 0.0313 and 0.0368 mim^{-1}, respectively.

BPA and RhB were also used to evaluate the photocatalytic performances of BiOI/ZSO-35 composite. As a comparison, pure BiOI and Zn_2SnO_4 were also tested under identical conditions. Figure 7 shows the BPA and RhB degradation curve under UV and visible light irradiation, respectively. As it can be seen, whatever under UV or visible light irradiation the degradation rates of BPA and RhB over BiOI/ZSO-35 was remarkably enhanced compared with pure BiOI and Zn_2SnO_4. For the BPA degradation, the physical mixture of BiOI and Zn_2SnO_4 (Labeled as PM-35wt.% BiOI/ZSO) was also used as a comparison. It can be clearly seen that the photocatalytic performance of BiOI/ZSO-35 was obviously higher than that of PM-35wt.% BiOI/ZSO. Under visible light irradiation, the degradation ratio of BPA was up to 99% after 180 min of reaction, while that over PM-35wt.% BiOI/ZSO was only 21%. Under UV light irradiation, the degradation rate of BPA was greatly accelerated, and about 97% of BPA was photocatalytical decomposed within 100 min of reaction. As for the degradation of RhB, a very similar phenomenon was observed.

The photocatalytic kinetic rate constants for the degradation of different pollutants were shown in Figure 8. It can be seen that the k for RhB photo-degradation over the BiOI/ZSO-35 catalyst under UV and visible light irradiation was about 2.1 and 8.4 times, 35 and 10 times higher than that over pure Zn_2SnO_4 and BiOI, respectively. The k for BPA photodegradation over the BiOI/ZSO-35 catalyst under UV and visible light irradiation was about 6 and 10 times, 53 and 37 times higher than that over pure Zn_2SnO_4 and BiOI, respectively.

These results indicated clearly that the activity enhancement of $BiOI/Zn_2SnO_4$ under UV and visible light irradiation may be due to the synergistic effect of heterojunction formed between Zn_2SnO_4 and BiOI accelerates separating electron-hole pairs at the interface.

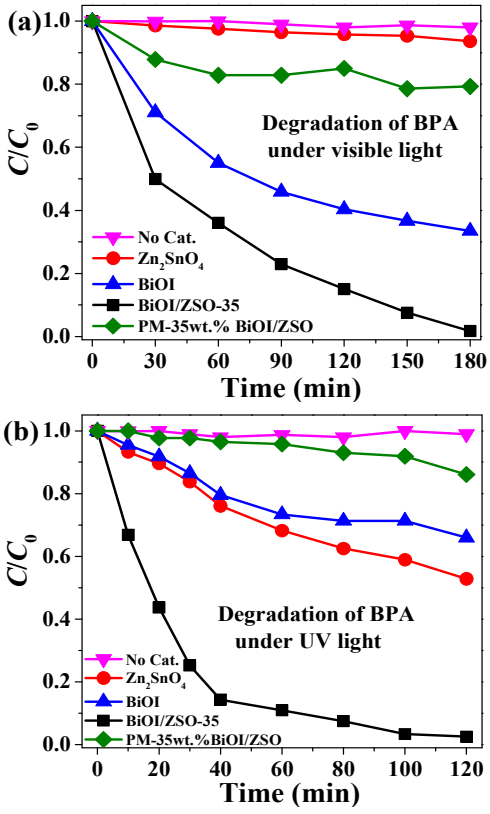

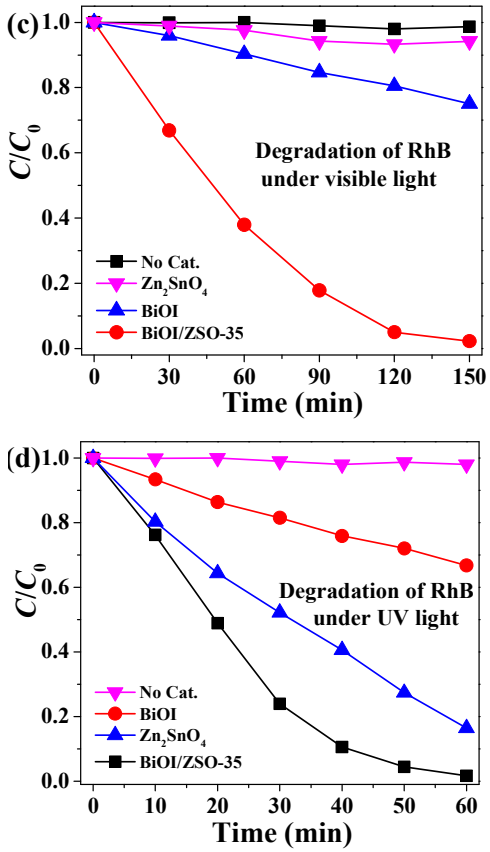

Figure 7. Photo-degradation activities of Zn_2SnO_4, BiOI, BiOI/ZSO-35, and PM-35wt.% BiOI/ZSO for the degradation of (a, b) BPA and (c, d) RhB under UV and visible light irradiation.

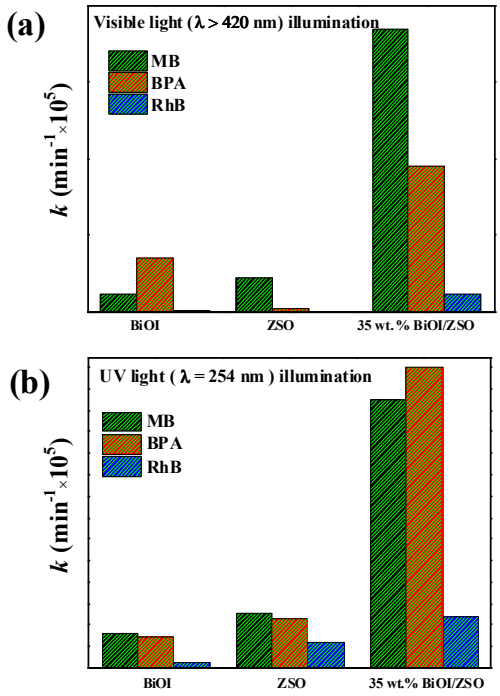

Figure 8. Photo-degradation rate constant *k* of MB, RhB and BPA upon BiOI/ZSO-35 under (a) visible ($\lambda > 420$ nm) light and (b) UV ($\lambda = 254$ nm) light irradiation.

Regeneration and reusability

To test the stability of $BiOI/Zn_2SnO_4$ composites for the photocatalytic degradation of MB, the catalyst recycled after reaction was reused for photocatalytic reaction five times under the same conditions and the results are shown in Figure 9. It can be seen that the photocatalytic efficiency does not exhibit any significant loss after five recycles, which indicate that the catalyst is stable for the photodegradation of MB. Additionally, the XRD patterns in Figure 10 reveal that there is no observable structural difference between the samples before and after reaction, indicating that the phase and structure of $BiOI/Zn_2SnO_4$ heterostructure remain intact and stable. These results indicate that the $BiOI/Zn_2SnO_4$ composite prepared by this facile method is stable and completely recyclable for the photocatalysis degradation of pollutant, which is important for its practical application.

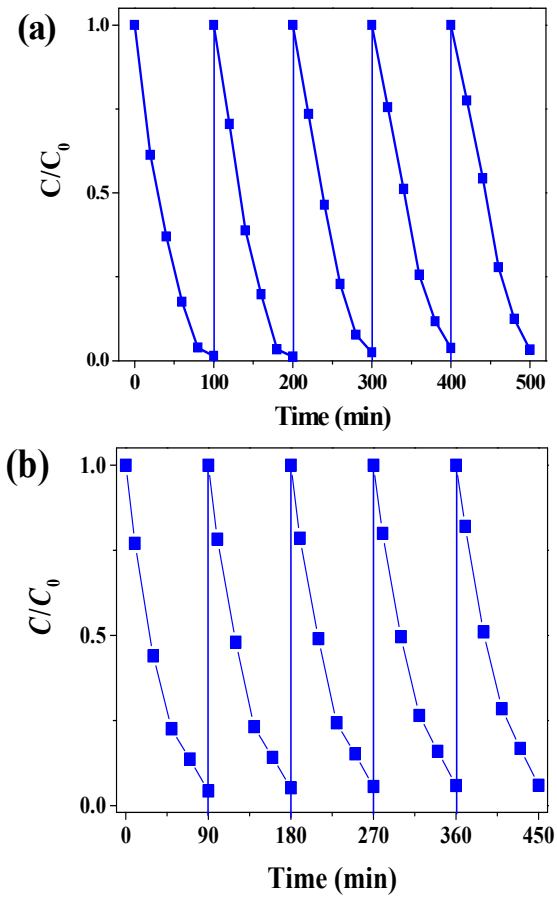

Figure 9. Recycling test on the BiOI/ZSO-35 composite for the degradation of MB under (a) visible ($\lambda > 420$ nm) light and (b) UV ($\lambda = 254$ nm) light irradiation.

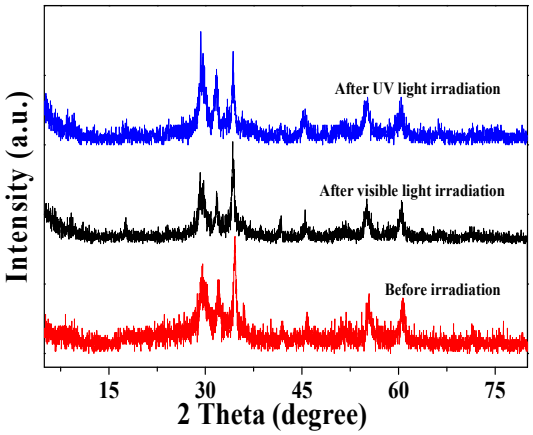

Figure 10. XRD patterns of the BiOI/ZSO-35 composite before and after photocatalytic reaction.

Possible photocatalytic mechanism

Separation efficiency of photo-generated electron-hole pairs

To investigate the interface charge separation efficiencies of BiOI/Zn_2SnO_4 composites, photocurrent and EIS characterizations have been carried out. As shown in Figure 11a, a fast photocurrent response can be observed for each switch-on and switch-off event in all the electrodes. The BiOI/Zn_2SnO_4 composites exhibit higher transient photocurrent intensity than that on single-component semiconductor, and the photocurrent changes tendency of the samples correspond to the photocatalytic performance variations. The transient photocurrent enhancements of the BiOI/Zn_2SnO_4 composites indicate the high separation rates of photo-induced electron–hole pairs. Among these, the BiOI/ZSO-35 composite exhibits the highest current intensity, demonstrating that a more effective separation of photon-generated carriers and faster interfacial charge transfer occurred in the BiOI/ZSO-35 composite. As shown in Figure 11b, the diameter of the Nyquist circle of BiOI/ZSO-35 composite was smaller than that of pure BiOI and Zn_2SnO_4, indicating that the BiOI/ZSO-35 composite had a relatively lower resistance compared with one-component catalyst. The results demonstrate that the effective transfer and separation of photo-induced carriers is critical factors to improve the activity of heterojunction.

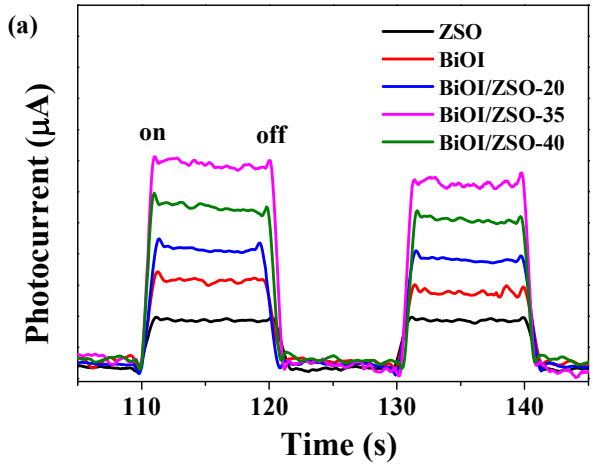

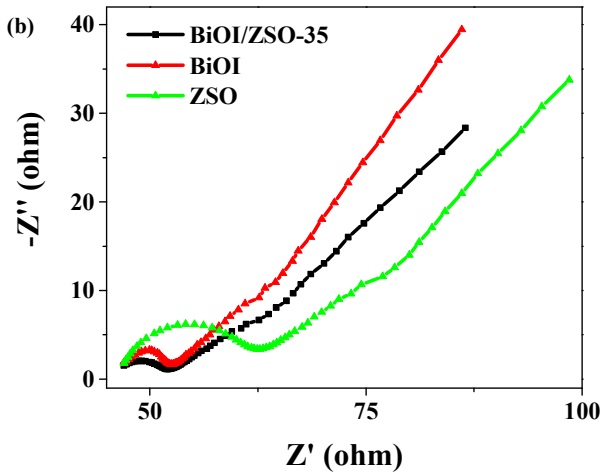

Figure 11. (a) Photocurrent responses and (b) EIS profiles of pure Zn_2SnO_4, BiOI, and BiOI/Zn_2SnO_4 composites under visible light irradiation.

Detection of active species

To investigate the photocatalytic degradation mechanism of pollutants over these heterostructured catalysts, diagnostic experiments have also been performed. Hence, various scavengers, such as *t*-BuOH (·OH scavenger) [40], $(NH_4)_2C_2O_4$ (AO) (h^+ scavenger) [41], *p*-benzoquinone (BQ) ($\cdot O_2^-$ scavenger), and NaN_3 ($^1O_2$ scavenger) [42], were introduced to evaluate the contributions of different active species on the photo-degradation efficiency. The photocatalytic degradation results in the presence of different scavengers under UV or visible light irradiation are shown in Fig. 12. When IPA (1.0 mL) was added, the degradation ratios of MB under visible and UV light illumination decreased to 70 and 60%, respectively. When AO (0.2 g) added, the degradation ratios decreased to 30 and 80% accordingly. Furthermore, the addition of BQ (0.05 g) or NaN_3 (0.05 g) could also decrease the photo-degradation rates of MB under the same reaction conditions. Summarizing the results above, the reactive species ·OH, $\cdot O_2^-$, h^+, and $^1O_2$ participated in the photo-degradation reaction and played equivalent role in the photocatalytic process under visible light irradiation. However, under UV light irradiation, the effect of h^+ and $^1O_2$ played vital important contributions, but the participation of ·OH and $\cdot O_2^-$ played a minor role for the MB degradation. In order to study the effect of molecular oxygen on the degradation of MB, N_2 was bubbled into the catalytic system to ensure that the reaction was

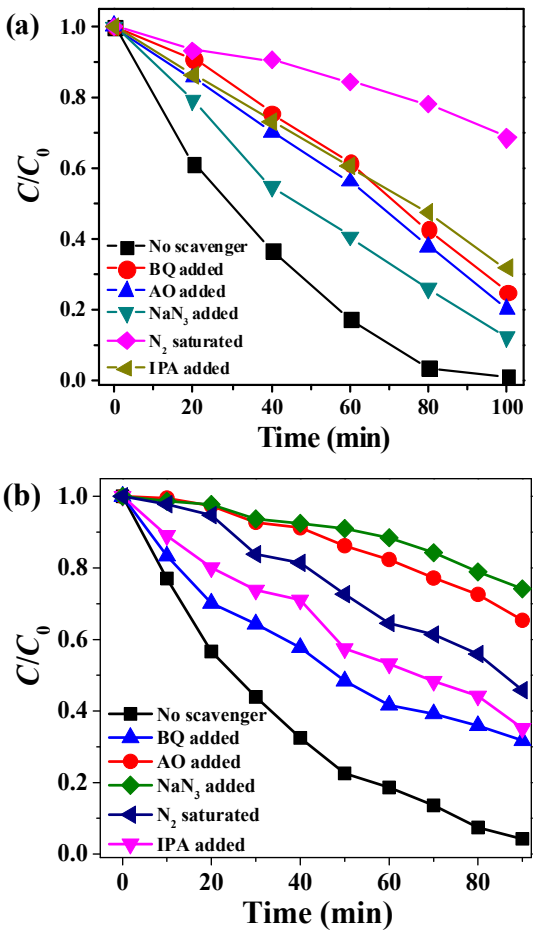

Figure 12. Effects of different scavengers on the degradation of MB in the presence of 35wt%BiOI/ZSO under (a) visible (λ>420 nm) and (b) UV (λ=254 nm) light irradiation.

operated without O_2 as an electron scavenger to produce a variety of active oxygen species. It shows that the degradation efficiency of MB decreased obviously, which meant that the molecular oxygen may play a non-ignorable role in the degradation process.

The proposed photocatalytic mechanism

In order to understand the band structures of BiOI/Zn_2SnO_4, the CB and VB positions of the materials were calculated by a simple theoretical method. The CB and VB positions were calculated through the equation:

$$E_{VB} = X - E^e + 0.5E_g$$

Where X is the Mulliken's electronegativity, E^e is the energy of free electrons on the hydrogen scale (4.50 eV), and E_g is the band gap [43]. The X values for Zn_2SnO_4 and BiOI were 7.0 and 5.94 eV, respectively. Accordingly, the top of VB and bottom of CB of Zn_2SnO_4 was calculated to be +4.3 and +0.7 eV (vs NHE), respectively. The VB and CB of BiOI was estimated to be +0.57 and +2.42 eV (vs NHE), respectively. When BiOI and Zn_2SnO_4 are in contact, since the CB potential of Zn_2SnO_4 is more negative than that of BiOI, the photo-generated electrons will transfer from Zn_2SnO_4 to BiOI, resulting in the accumulation of negative charges in BiOI close to the junction. Meanwhile, the photo-generated holes transfer from BiOI to Zn_2SnO_4, leaving a positive section in Zn_2SnO_4 near the junction. With equilibration of BiOI and Zn_2SnO_4 Fermi levels (E_f), the diffusion of electrons from Zn_2SnO_4 to BiOI stops. At the same time, the energy bands of BiOI shift upward along the Fermi level ($E_{f\text{-}p}$) and those of the Zn_2SnO_4 shift downward along its Fermi level ($E_{f\text{-}n}$), as shown in scheme 1.

Under visible light irradiation, only BiOI could be excited to generate electron–hole pairs. Due to the effect of the internal field with the direction from Zn_2SnO_4 to BiOI, the photoelectrons on the CB of BiOI efficiently transferred to that of Zn_2SnO_4, and holes remained on the VB of BiOI. Under UV light irradiation, both BiOI and Zn_2SnO_4 absorb photons of energy greater than the corresponding band gap energy, which excite the electrons in the VB to the CB and leave holes in the VB. The photo-generated electrons in the CB of BiOI are then transferred to the CB of Zn_2SnO_4, and the photo-generated holes in the VB of Zn_2SnO_4 transferred to the VB of BiOI. Therefore, the photo-generated electron–hole pairs will be effectively separated due to the formation of a junction between the BiOI and Zn_2SnO_4 interface, resulting in a suppressed electron–hole recombination.

The migration of photo-generated carriers can be promoted by the inner electric field established at the heterojunction interfaces. The photoelectrons were further trapped by molecular oxygen [44] to produce $\cdot O_2^-$ or ·OH reactive species [45]. Meanwhile, the photo-generated holes would decompose the pollutants adsorbed on the surface of the composite or react with $\cdot O_2^-$ to form $^1O_2$ reactive species, which continue participate in the degradation reaction.

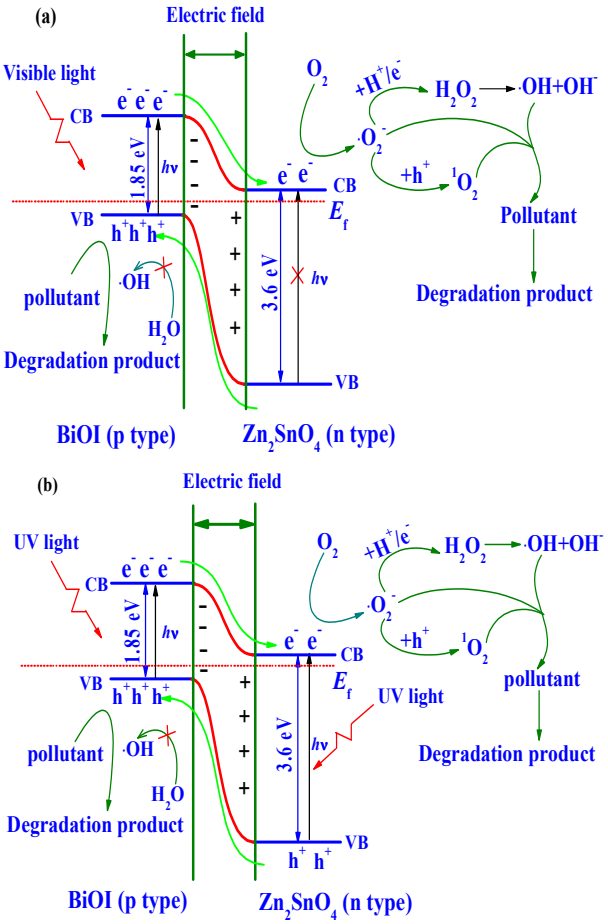

Scheme 1. Photocatalytic degredation mechanism over BiOI/Zn_2SnO_4 heterostructure under (a) visible and (b) UV light irradiation.

Conclusions

$BiOI/Zn_2SnO_4$ composites with different mass ratios have been synthesized via a facile chemical deposition method. The absorption edge of the $BiOI/Zn_2SnO_4$ heterojunction shifted significantly to longer wavelengths compared to Zn_2SnO_4. The BiOI/ZSO-35 composite shows excellent photocatalytic activities in the degradation of MB, RhB, and BPA under visible or UV light irradiation, respectively. The formation of heterostructure with intimate contacts between Zn_2SnO_4 and BiOI resulted in the easier charge transfer and more efficient separation of electron–hole pairs, which finally improved the photocatalytic activities of the composites. This study provides a simple and economical route to couple two different semiconductors with different physicochemical properties for developing novel high-performance photocatalysts.

Acknowledgment

This work was financially supported by the National Natural Science Foundation of China (No. 21271027, 21103069, and 40672158), the 863 Project of China (No. 20140AA065103-1), Scientific Research Reward Fund for Excellent Young and Middle-Aged Scientists of Shandong Province (BS2012HZ001), and Scientific Research Foundation for Doctors of University of Jinan (XBS1037, XKY1321, and XKY1043).

References

1 A. Fujishima and K. Honda, *Nature* 1972, **238**, 37.
2 Z. Zou, J. Ye, K. Sayama and H. Arakawa, *Nature* 2001, **414**, 625.
3 M. Xie, L. Jing, J. Zhou, J. Lin and H. Fu, *J. Hazard. Mater.* 2010, **176**, 139.
4 M. Shannon, P. Bohn, M. Elimelech, J. Georgiadis, B. Mari as and A. Mayes, *Nature* 2008, **452**, 301.
5 D. Yamasita, T. Takata, M. Hara, J.N. Kondo and K. Domen, *Solid State Ionics* 2004, **172**, 591.
6 R. Asahi, T. Morikawa, T. Ohwaki, K. Aoki and T. Taga, *Science* 2001, **293**, 269.
7 H.G. Yang, C.H. Sun, S.Z. Qiao, J. Zou, G. Liu, S.C. Smith, H.M. Cheng and G.Q. Lu, *Nature* 2008, **453**, 638.
8 X.S. Liu, J.Q. Wang, E.J. Liang and W.F. Zhang, *Appl. Surf. Sci.* 2013, **280**, 556.
9 K. Wang, Y. Huang, H.J. Huang, Y. Zhao, X.L. Qin, X. Sun and Y.L. Wang, *Ceram. Int.* 2014, **40**, 8021.
10 X. Y. Liu, H.W. Zheng, Z.L. Zhang, X.S. Liu, R.Q. Wan and W.F. Zhang, *J. Mater. Chem.* 2011, **21**, 4108.
11 M. Peiteado, Y. Iglesias, J.F. Fern´andez, J.De. Frutos and A.C. Caballero, *Mater. Chem. Phys.* 2007, **101**, 1.
12 E.L. Folettoa, J.M. Sim, M.A. Mazutti, S.L. Jahn and E.I. Muller, *Ceram. Int.* 2013, **39**, 4569.
13 X.B. Chen, S.H. Shen, L.J. Guo and S.S. Mao, *Chem. Rev.* 2011, **110**, 6503.
14 L. Chen, J. He, Q. Yuan, Y. Liu, C. T. Au and S.F. Yin, J. Mater. Chem. A 2015, DOI: 10.1039/c4ta05346j.
15 M. Xiong, L. Chen, Q. Yuan, J. He, S. L. Luo, C. T. Au, and S. F. Yin, Dalton Trans. 2014, 43, 8331.
16 J. Di, J. X. Xia, S. Yin, H. Xu, M. Q. He, H. M. Li, L. Xu, Y. P. Jiang, RSC Adv. 2013, 3, 19624.
17 J. Di, J. X. Xia, S. Yin, H. Xu, Y. G. Xu, M. Q. He, H. M. Li, J. Mater. Chem. A 2014, 2, 5340.
18 L. Chen, Q. Zhang, R. Huang, S. F. Yin, S. L. Luo and C. T. Au, Dalton Trans. 2012, 41, 9513.
19 L. Chen, S. F. Yin, S. L. Luo, R. Huang, T. Hong, C. T. Au, Ind. Eng. Chem. Res. 2012, 51, 6760.
20 J.X. Xia, S. Yin, H.M. Li, H. Xu, L. Xua and Q. Zhang, *Colloids and Surfaces A: Physicochem. Eng. Aspects* 2011, **387**, 23.
21 Y.Y. Li, J.S. Wang, H.C. Yao, L.Y. Dang and Z.J. Li, *J. Mol. Catal. A: Chem.* 2011, **334**, 116.
22 R. Hao, X. Xiao, X.X Zuo, J.M. Nan and W.D. Zhang, *J. Hazard. Mater*. 2012, **209-210**, 137.
23 G.P. Dai, J.G. Yu and G. Liu, *J. Phys. Chem. C* 2011, **115**, 7339.
24 X. Zhang, L.Z. Zhang, T.F. Xie and D.J. Wang, *J. Phys. Chem. C* 2009, **113**, 7371.
25 H.Q. Li, Y.M. Cui, W.S. Hong and B.L. Xu, *Chem. Eng. J.* 2013, **228**, 1110.
26 K.H. Reddy, S. Martha and K.M. Parida, *Inorg. Chem.* 2013, **52**, 6390.
27 J. Jiang, X. Zhang, P.B. Sun and L.Z. Zhang, *J. Phys. Chem. C* 2011, **115**, 20555.
28 H.R. Li, Z. Jin, H.G. Sun, L.M. Sun, Q.B. Li, X. Zhao, C.J. Jia and W.L. Fan, *Mater. Res. Bull.* 2014, **55**, 196.
29 J. Cao, B.Y. Xu, B.D. Luo, H.L. Lin and S.F. Chen, *Catal. Commun.* 2011, **13**, 63.
30 X.D. Lou, X.H. Jia, J.Q. Xu, S.Z Liu and Q.H. Gao, *Mater. Sci. Eng. A* 2006*,* **432**, 221.
31 J. Jiang, X. Zhang, P.B. Sun, and L.Z. Zhang, *J. Phys. Chem. C* 2011, **115**, 20555.
32 K. Kim, A. Annamalai, S.H. Park, T.H. Kwon, M.W. Pyeon and M.J. Lee, *Electrochim. Acta* 2012, **76,** 192.
33 Y.Y. Li, J.S. Wang, H.C. Yao, L.Y. Dang and Z.J. Li, *J. Mol. Catal. A: Chem.* 2011, **334**, 116.
34 X. Zhang and L.Z. Zhang, *J. Phys. Chem. C* 2010, **114**, 18198.
35 X. Fu, X. Wang and J. Long, *J. Solid State Chem.* 2009 **182(3)**, 517.
36 X. Zhang, Z.H. Ai, F.L. Jia and L.Z. Zhang, *J. Phys. Chem. C* 2008, **112**, 747.
37 J. Cao, B.Y. Xu, H.L. Lin, B.D. Luo and S.F. Chen, *Chem. Eng. J.* 2012, **185(186)**, 91.
38 H.Lin, S.Liao and S.Hung, *Mater. Chem. Phys.* 2009, **117(1)**, 9.
39 J. Cao, B.Y. Xu, H.L. Lin and S.F. Chen, *Chem. Eng. J.* 2013, **228**, 482.
40 Y. Hu, D.Z. Li, Y. Zheng, W. Chen, Y.H. He, Y. Shao, X.Z. Fu and G.C. Xiao, *Appl. Catal. B: Environ.* 2011, **104**, 30.
41 J. Cao , B.Y. Xu, H.L. Lin , B.D Luo and S.F Chen, *Catal. Commun.* 2012, **20**, 204.
42 C. Chang, L.Y. Zhu, Y. Fu and X.L. Chu, *Chem. Eng. J.* 2013, **233**, 305.
43 Y. Xu and M. A. A. Schoonen, *Am. Mineral.* 2000, 85, 543.
44 H.F. Cheng, B.B. Huang, X.Y. Qin, X.Y. Zhang and Y. Dai, *Chem. Commun.* 2012, **48**, 97.
45 L. Chen, R. Huang, S.F. Yin, S.L. Luo and C.T. Au, *Chem. Eng. J.* 2012, **193-194**, 123.